Electronic Supplementary Information (ESI) for J. Mater. Chem. A

Yolk−Shell Structured Metal–Organic Framework with Encapsulated Iron-Porphyrin and Its Derived Bimetallic Nitrogen-Doped Porous Carbon for Efficient Oxygen Reduction Reaction

Chaochao Zhang,[†, a] Hao Yang,[†, b] Dan Zhong,[†, c] Yang Xu,[a] Yanzhi Wang,[a] Qi Yuan,[b] Zuozhong Liang,[a] Bin Wang,[a] Wei Zhang,[a] Haoquan Zheng,*[a] Tao Cheng,*[b] and Rui Cao*[a]

[a.] Key Laboratory of Applied Surface and Colloid Chemistry, Ministry of Education, School of Chemistry and Chemical Engineering, Shaanxi Normal University, Xi'an 710119, China.

[b.] Institute of Functional Nano and Soft Materials (FUNSOM), Jiangsu Key Laboratory for Carbon-Based Functional Materials and Devices, Soochow University, Suzhou 215123, China.

[c.] Zhuhai Da Hengqin Science and Technology Development Co., Ltd, Hengqin New Area, Zhuhai 519000, China

Email: zhenghaoquan@snnu.edu.cn; tcheng@suda.edu.cn; ruicao@ruc.edu.cn

† These authors contributed equally to this work.

Keywords: Iron-porphyrin; yolk–shell structure; metal–organic framework; nitrogen-doped porous carbon; oxygen reduction reaction.

S1. Experimental Section

***Chemical and Material*:** Hmim (98%), $Co(NO_3)_2·6H_2O$ (99.99%), $Zn(NO_3)_2·6H_2O$ (99.99%) are purchased from the Energy Chemical. 5,10,15,20-Tetraphenylporphyrinatoiron (FeTPP) is prepared according to the literature.

Synthesis of 5,10,15,20-Tetraphenylporphyrin (TPP): 4 mL of Benzaldehyde was dissolved in 150 mL of propionic acid. Then, 2.8 mL of pyrrole was added into the solution. The above solution was heated to 140 °C and kept under stirring for 1 h. The mixture was cooled to room temperature, filtered, and washed with methanol until the methanol washings were colorless. The resultant purple solid was dried in high vacuum to obtain pure TPP.

Synthesis of 5,10,15,20-Tetraphenylporphyrinatoiron (FeTPP): 200 mg of TPP and 20 mL of *N*,*N*-dimethylformamide were added in Shrek bottle. Then, 1 g of $FeCl_2·4H_2O$ was added into the solution. The solution was degassed and refilled with Ar for 0.5 h. The solution was refluxed for 1 h and cooled to room temperature. 100 mL of DI water was then added. Finally, the FeTPP solid was collected by suction filtration, washed with deionized water, and dried by high vacuum.

Preparation of the Working Electrode:

The catalyst ink for ORR tests was prepared as following: 4 mg of catalysts was dispersed into a mixed solution of 490 μL of deionized water, 490 μL of ethanol and 20 μL of Nafion solution, then ultrasonicated for 30 min to obtain a homogeneous solution. 20 μL of the catalysts ink is dropped on the RDE electrode and dried slowly at room temperature. The final mass loading of the catalysts on electrode is around 0.08 mg.

The catalyst ink for OER tests was prepared as following: 4 mg of catalysts was dispersed into a mixed solution of 667 μL of deionized water, 333 μL of ethanol and 30 μL of Nafion solution, then ultrasonicated for 30 min to obtain a homogeneous solution. 5 μL of the catalysts ink is dropped on the GC electrode and dried slowly at room temperature. The final mass loading of the catalysts on electrode is around 0.28 mg cm^{-2}.

ORR measurement details: The potentials corresponding to the reversible hydrogen electrode (RHE) electrode was calculated with the following equation:

$$E_{RHE} = E_{Ag/AgCl} + (0.197 + 0.059 \times \mathrm{pH})$$

The electron transfer numbers (*n*) was calculated with Koutecky-Levich (K-L) equation:

$$\frac{1}{j} = \frac{1}{j_l} + \frac{1}{j_k} = \frac{1}{B\omega^{1/2}} + \frac{1}{j_k}$$

where j is the measured current density; j_l is the diffusion current density; j_k is the kinetic current density; ω is the rotation speed in rpm; B can be confirmed by Koutecky-Levich (K-L) equation:

$$\mathrm{B} = 0.2\mathrm{nFC_0}(D_0)^{2/3}\upsilon^{-1/6}$$

where n is the transfer numbers; F is the Faraday constant (96485 C mol^{-1}); C_0 is the concentration of O_2 in 0.1 M KOH (1.2×10^{-6} mol cm^{-3}); D0 is the diffusion coefficient of O_2 in 0.1 M KOH (1.9×10^{-5} cm^2 s^{-1}); υ is the viscosity of 0.1 M KOH (0.1 cm^2 s^{-1}). Afterwards, the transfer number (n) can be obtained by the equation.

The electron transfer number can be obtained by another equation:

$$\mathrm{n} = 4\frac{i_d}{i_d + i_r/N}$$

i_d is the disk current; i_r is the ring current; N is the capture coefficient and it is about 0.37. the percentage of hydrogen peroxide produced can be confirmed by the following equation:

$$H_2O_2\% = 200\frac{i_r/N}{i_d + i_r/N}$$

OER measurement details: The potentials corresponding to the reversible hydrogen electrode (RHE) electrode was calculated with the following equation:

$$E_{RHE} = E_{Ag/AgCl} + (0.197 + 0.059 \times \text{pH})$$

The overpotentials (η) was calculated with the following equation:

$$\eta = E_{RHE} - 1.23$$

Simulation Details: We reduced the several nanometers size of Co-embedded N–doped graphitic carbon structures to a single layer N-doped graphene which adsorbed on fcc Co (111) slab to represent the Co–C/N surface, which we consider well represents the experiment as well as keeping the computational cost affordable. The Co metal part consists of x by x by four-layer slab model with a vacuum region of 15 Å in the z direction. The in-plane lattice parameters are 2.46 Å of graphene and 2.51 Å of Co, which are close enough to lead to ignorable surface mismatch within 1%. The simulated system consists of 4×4 supercells of graphene and one Co. Four pyridinic-type N atoms uniformly replace the C in the graphene lattice, leading to a percentage of 6 % with respect to C, which is close to the experimental observation. The metal site of Co–N_4 is Co coordinated with four adjacent N atoms, and the metal site of FeCo–C/N is Fe coordinated with four adjacent N atoms.

To predict the ORR activities on two different models, we calculated the adsorption free energies of three oxygenated intermediate species, including OOH^*, OH^* and O^*. The energy differences of these reactions are derived from the calculated adsorption energies of these oxygenated intermediate species. Zero-point energies (ZPE), entropy corrections are considered in all these cases, and the Gibbs free energies are given by

$$\Delta G = \Delta E_{\mathrm{DFT}} + \Delta \mathrm{ZPE} - \mathrm{T}\Delta S \tag{1}$$

where ΔE_{DFT}, ΔZPE and ΔS are the change of DFT total energy, zero-point energy, and entropy from the initial to the final state;

The effects of applied voltage is considered by including the eU term.

$$\Delta G^U = \Delta G + eU \tag{2}$$

U is the electrode potential, and e is the electron transferred. The reference potential is standard hydrogen electrode.[1]

Characterization: The morphology of the catalysts was obtained with the field emission scanning electron microscopy (FESEM, Hitachi, SU8220) and the field emission transmission electron microscopy (FETEM, FEI, Tecnai G2 F20;). EDS analysis was conducted on an AMETEK Materials Analysis EDX equipped on the TEM. PXRD patterns of the catalysts were measured with a X-ray diffractometer (Bruker, D8 Advance, Cu Kα, λ = 1.5406 Å, 40 kV/40mA). The Raman spectrum were measured with a Raman Spectrometer (Renishaw, in Via Reflex). The BET specific surface area was tested in Micromeritics ASAP 2020. The XPS analysis of the prepared catalysts was performed with a Kratos AXIS ULTRA XPS.

S2. Characterizations and Results

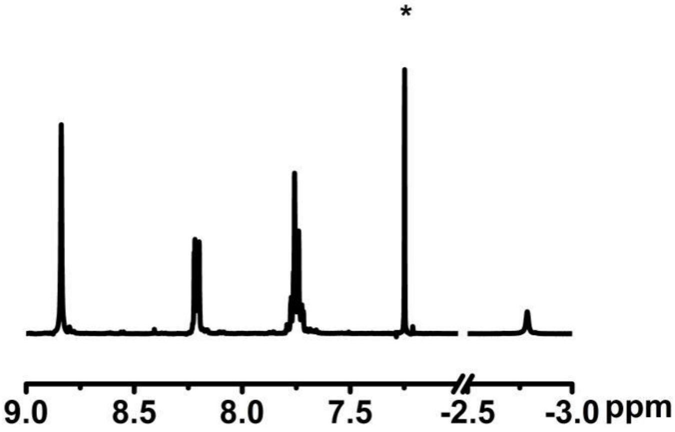

Fig. S1. 1H NMR spectrum of 5,10,15,20-Tetraphenylporphyrin (TPP) in $CDCl_3$. The solvent residue peak is labeled (*).

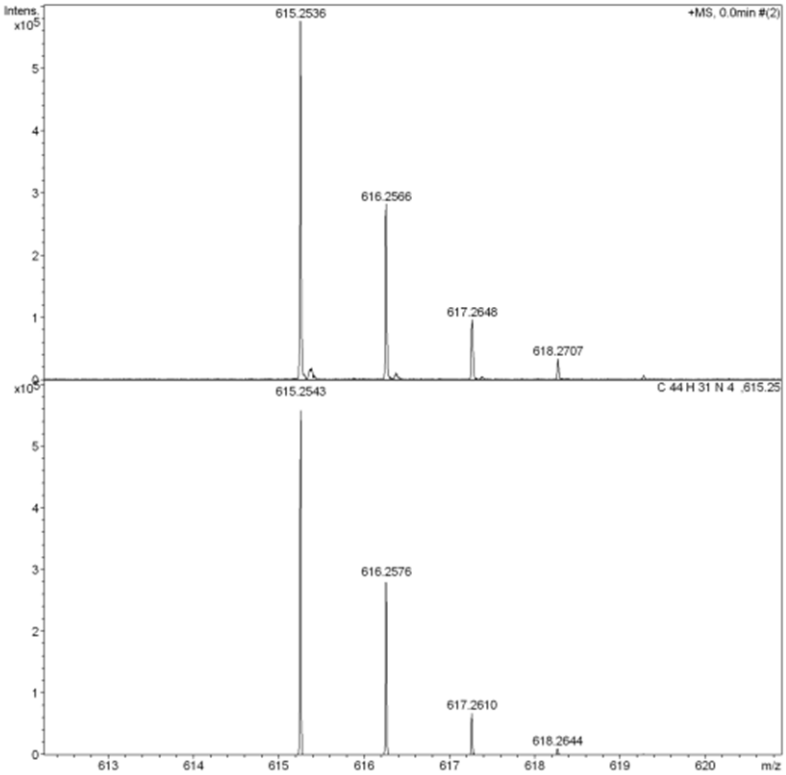

Fig. S2. The LC-MS mass spectra of 5,10,15,20-Tetraphenylporphyrin (TPP).

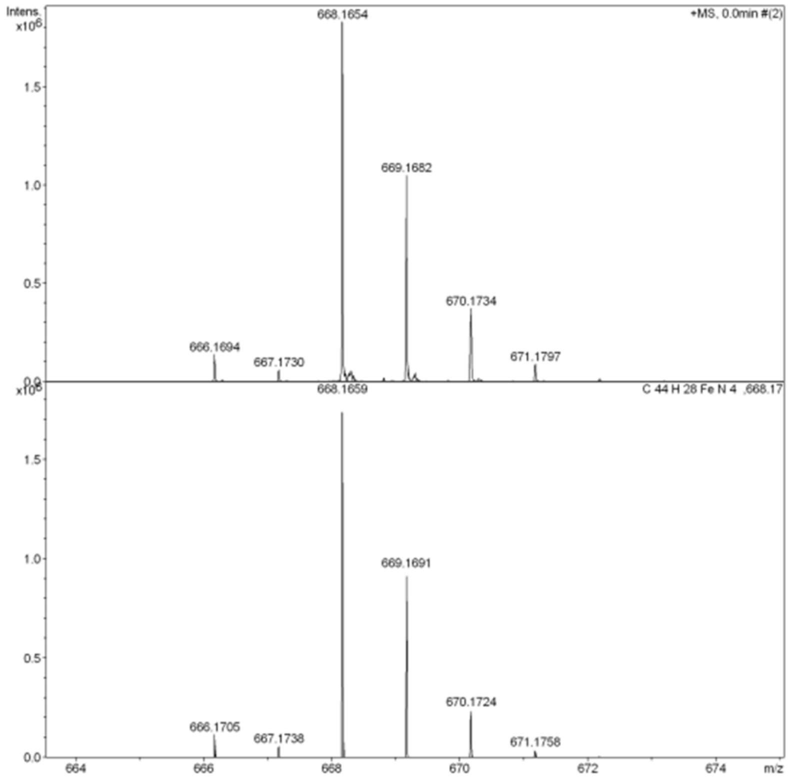

Fig. S3. The LC-MS mass spectra of 5,10,15,20-Tetraphenylporphyrinatoiron (FeTPP).

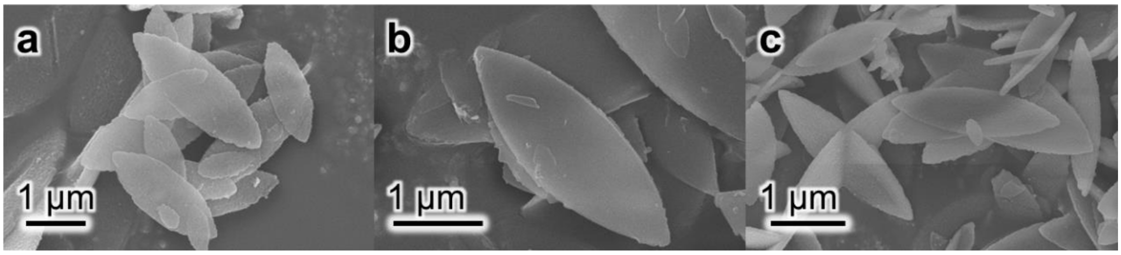

Fig. S4. SEM images of a) ZIF-L; b) ZIF-L@ZIF-8; c) ZIF-L&FeTPP@ZIF-8.

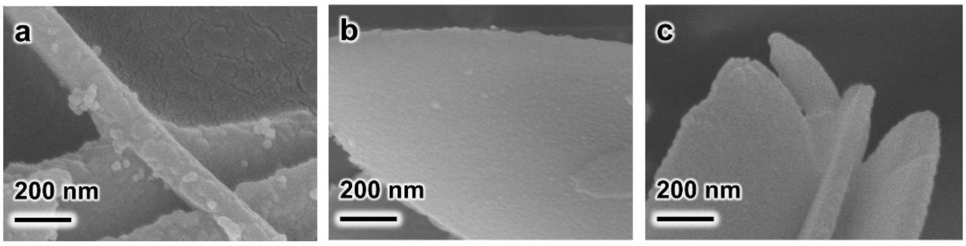

Fig. S5. SEM images of ZIF-L&FeTPP@ZIF-8 with different dosages of Zn ions and Hmim. a) 0.6 mmol $Zn(NO_3)_2 \cdot 6H_2O$ + 4.8 mmol Hmim; b) 0.5 mmol $Zn(NO_3)_2 \cdot 6H_2O$ + 4 mmol Hmim; c) 0.4 mmol $Zn(NO_3)_2 \cdot 6H_2O$ + 3.2 mmol Hmim.

ZIF-8 can be carefully controlled to form this yolk-shell structured ZIF-L&FeTPP@ZIF-8. As shown in Figure, there are a lot of small particles on the outer surface of ZIF-L&FeTPP@ZIF-8-Fe or dispersed in solution using a high concentration of Zn ions and Hmim.

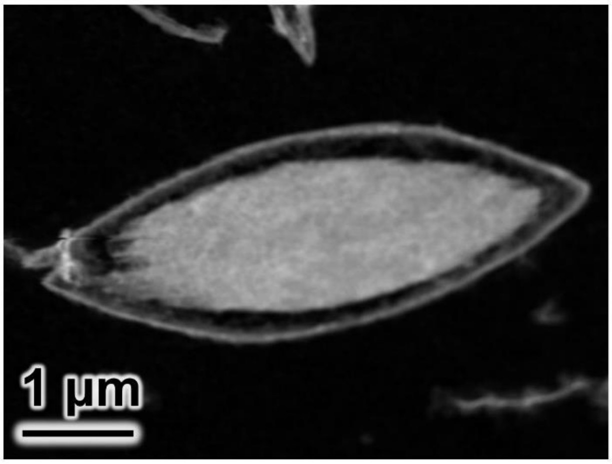

Fig. S6. The High-angle annular dark field-scanning transmission electron microscopy (HAADF-STEM) of ZIF-L&FeTPP@ZIF-8.

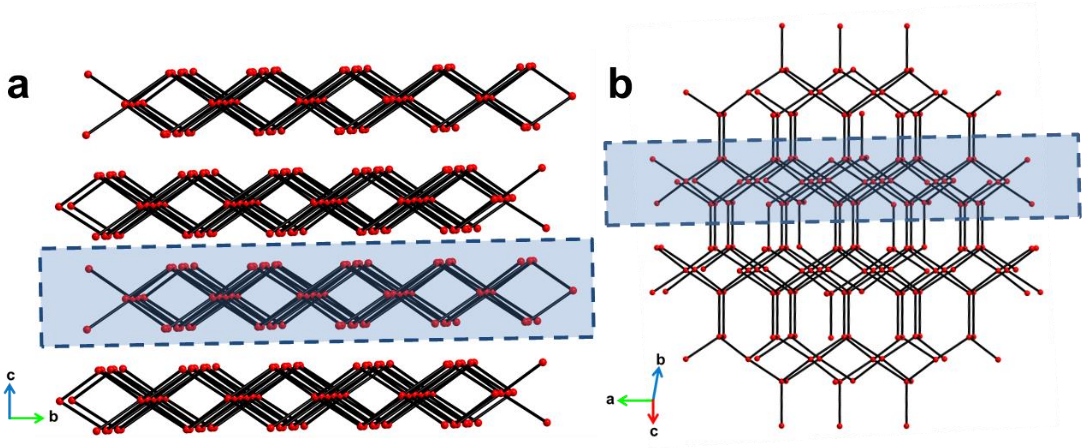

Fig. S7. The topological structure of (a) ZIF-L and (b) ZIF-8. Only the network of the Zn atoms is shown.

Relationship between ZIF-L and ZIF-8: ZIF-8 framework with a sodalite cage and the layer corresponding to ZIF-L. The same building units in ZIF-L and ZIF-8 are highlighted.

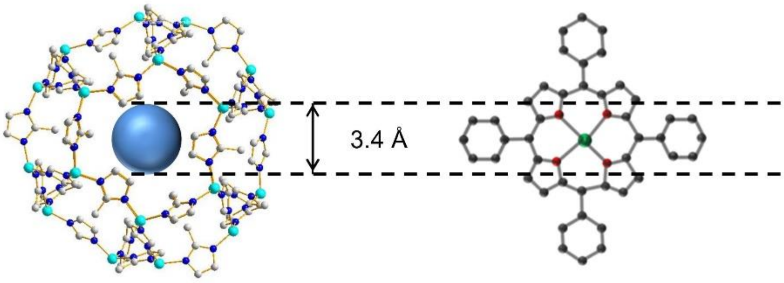

ZIF-8 framework FeTPP molecule

Fig. S8. The comparison of the molecular size of FeTPP and the size of pore aperture of ZIF-8 framework.

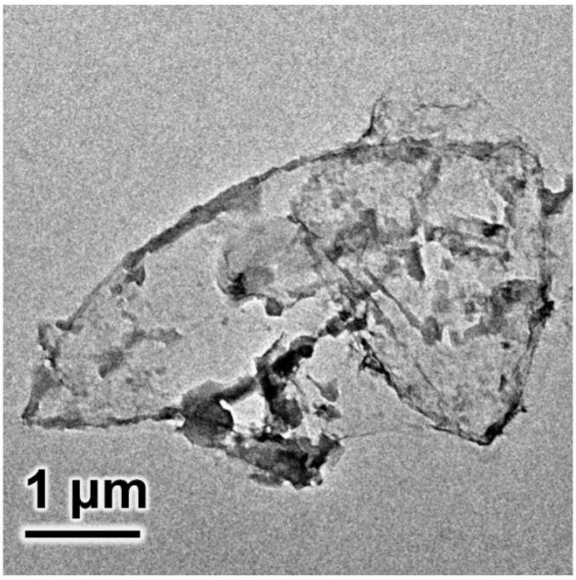

Fig. S9. The TEM image of ZIF-L after stirring for 24 hours in the solution of FeTPP.

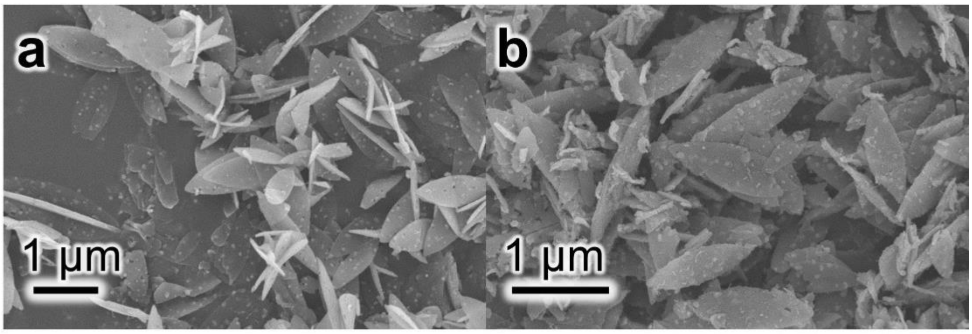

Fig. S10. SEM images of a) Co-C/N-1; b) Co-C/N-2.

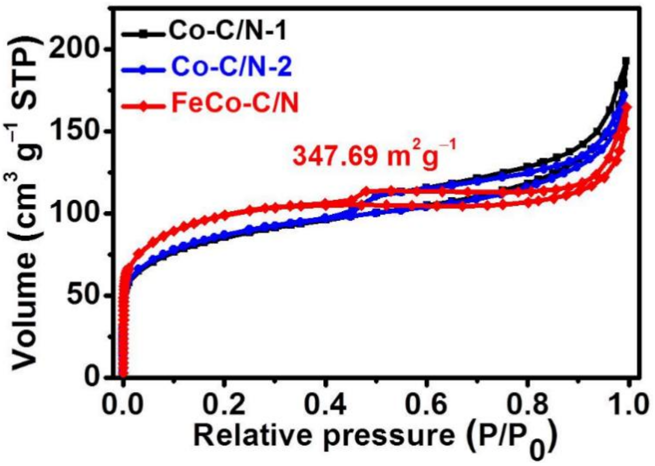

Fig. S11. N_2 adsorption/desorption curves of Co-C/N-1,Co-C/N-2, FeCo-C/N.

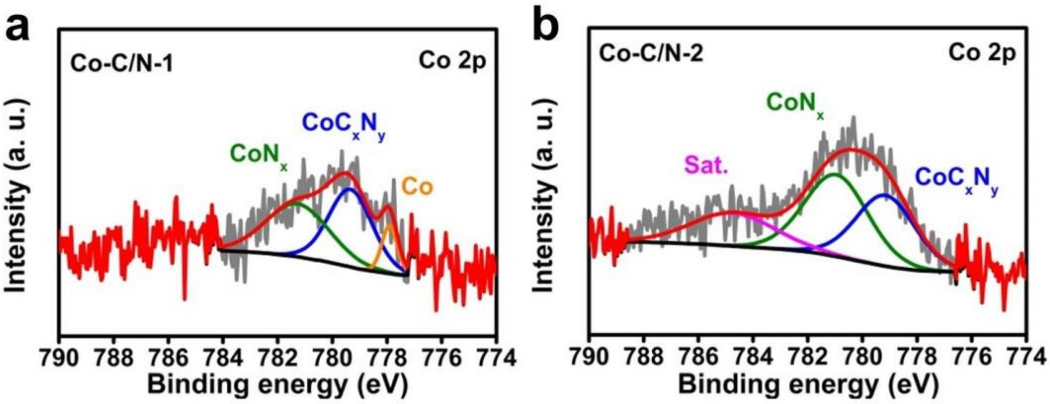

Fig. S12. High-resolution XPS spectra of Co 2p for Co-C/N-1 (a) and Co-C/N-2 (b).

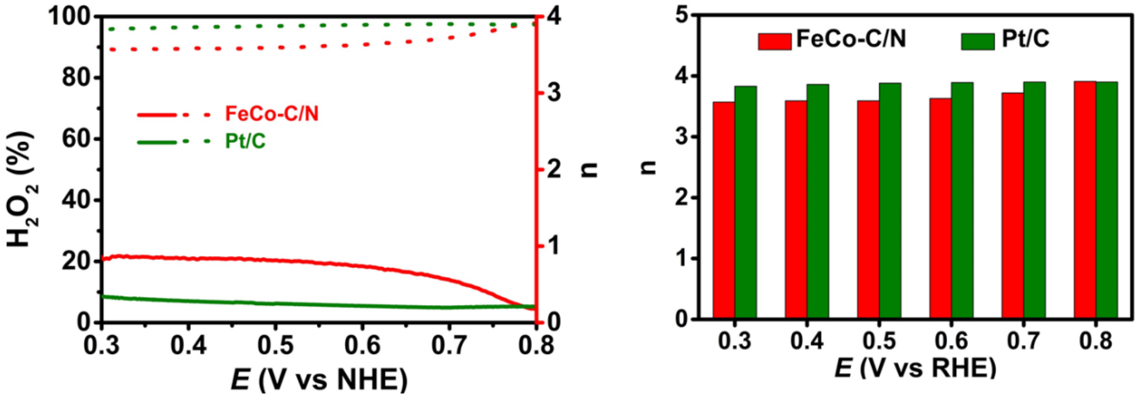

Fig. S13. a) peroxide yield as well as the calculated electron transfer numbers (*n*) of Pt/C (green) and FeCo-C/N (red). b) the electron transfer numbers of FeCo-C/N and Pt/C at different potential.

Table S1. The percentage of different kinds of N in different catalysts.

	Graphitic N	Pyrrolic N	Pyridinic N
FeCo-C/N	13.65 %	36.09 %	50.26 %
Co-C/N-1	29.20 %	44.41 %	26.39 %
Co-C/N-2	20.48 %	31.01 %	48.51 %

Table S2. The electron transfer numbers under different conditions.

Catalysts	0.8 V	0.7 V	0.6 V	0.5 V	0.4 V	0.3 V
FeCo-C/N	3.91	3.72	3.63	3.59	3.59	3.57
Pt/C	3.90	3.90	3.89	3.88	3.86	3.83

Table S3. Comparison of the ORR performance of Co-N-C catalysts from literature and this work

Catalyst	Electrolyte	$E_{1/2}$ vs RHE	Ref.
FeCo-C/N	**0.1M KOH**	**864 mV**	**This work**
FeCo‑DHO/NCNTs	0.1 M KOH	860 mV	[2]
Fe_3C-Co/NC	0.1 M KOH	830 mV	[3]
CoZn-NC-700	0.1 M KOH	840 mV	[4]
Co_2P/CoN-in-NCNTs	0.1 M KOH	850 mV	[5]
NiFeLDH/Co,N-CNF	0.1 M KOH	790 mV	[6]
N-Co_3O_4@NC-2	0.1 M KOH	770 mV	[7]
MnO/Co/PGC	0.1 M KOH	780 mV	[8]
NC-Co_3O_4-90	0.1 M KOH	870 mV	[9]
Co_3O_4-NP/N-rGO	0.1 M KOH	750 mV	[10]
Co-CoO/N-rGO	0.1 M KOH	780 mV	[11]

Table S4. Adsorption energies of ORR reaction intermediates for FeCo-C/N and Co-C/N models, respectively.

	Adsorption energy (in eV)	
	FeCo-C/N	Co-C/N
*O	−4.066	−2.759
*O_2	−0.806	−0.499
*OH	−2.700	−2.328
*OOH	−1.133	−0.789

Table S5. The calculated formation energies of elementary reactions of ORR on the FeCo-C/N and Co-C/N models.

Reaction process	$\Delta G_{\text{FeCo-C/N}}$ (eV)	$\Delta G_{\text{Co-C/N}}$ (eV)
$\star O_2 + H_2O + e^- \rightarrow \star OOH + OH^-$	−0.458	−0.406
$\star OOH + e^- \rightarrow \star O + OH^-$	−1.562	−1.042
$\star O + H_2O\ (l) + e^- \rightarrow \star OH + OH^-$	−1.327	−1.915
$\star OH + e^- \rightarrow \star + OH^-$	−0.767	−1.058

Table S6. Comparison of Zn-air performance of different catalysts from literature and this work.

Electrode	Power Density (mW cm^{-2})	OCV (V)	Ref.
FeCo-C/N	397.25	1.519	This work
Co/Co-N-C	132	-	[12]
GNCNTs-4	253	1.48	[13]
Co-N_x/C NRA	193.2	1.42	[14]
FeN_x/C-700-20	36	1.6	[15]
Co/Co_3O_4@PGS	118.27	1.45	[16]
MnO/Co/PGC	172	1.42	[8]
$Fe_{0.5}Co_{0.5}O_x$/NrGO	86	1.43-1.44	[17]
NGM-GO	152	1.439	[18]
CoNiFe-S MNs	140	-	[19]

References

[1] J. Rossmeisl, Z. W. Qu, H. Zhu, G. J. Kroes, J. K. Nørskov, *J. Electroanal. Chem.* **2007**, *607*, 83.
[2] M. Wu, Q. Wei, G. Zhang, J. Qiao, M. Wu, J. Zhang, Q. Gong, S. Sun, *Adv. Energy Mater.* **2018**, *8*, 1801836.
[3] C. C. Yang, S. F. Zai, Y. T. Zhou, L. Du, Q. Jiang, *Adv. Funct. Mater.* **2019**, *29*, 1901949.
[4] B. Chen, X. He, F. Yin, H. Wang, D.-J. Liu, R. Shi, J. Chen, H. Yin, *Adv. Funct. Mater.* **2017**, *27*, 1700795.
[5] Y. Guo, P. Yuan, J. Zhang, H. Xia, F. Cheng, M. Zhou, J. Li, Y. Qiao, S. Mu, Q. Xu, *Adv. Funct. Mater.* **2018**, *28*, 1805641.
[6] Q. Wang, L. Shang, R. Shi, X. Zhang, Y. Zhao, G. I. N. Waterhouse, L.-Z. Wu, C.-H. Tung, T. Zhang, *Adv. Energy Mater.* **2017**, *7*, 1700467.
[7] Z. Wang, W. Xu, X. Chen, Y. Peng, Y. Song, C. Lv, H. Liu, J. Sun, D. Yuan, X. Li, X. Guo, D. Yang, L. Zhang, *Adv. Funct. Mater.* **2019**, *29*, 1902875.
[8] X. F. Lu, Y. Chen, S. Wang, S. Gao, X. W. D. Lou, *Adv. Mater.* **2019**, *31*, e1902339.
[9] C. Guan, A. Sumboja, H. Wu, W. Ren, X. Liu, H. Zhang, Z. Liu, C. Cheng, S. J. Pennycook, J. Wang, *Adv. Mater.* **2017**, *29*, 1704117.
[10] X. Han, G. He, Y. He, J. Zhang, X. Zheng, L. Li, C. Zhong, W. Hu, Y. Deng, T.-Y. Ma, *Adv. Energy Mater.* **2018**, *8*, 1702222.
[11] X. Liu, W. Liu, M. Ko, M. Park, M. G. Kim, P. Oh, S. Chae, S. Park, A. Casimir, G. Wu, J. Cho, *Adv. Funct. Mater.* **2015**, *25*, 5799.
[12] P. Yu, L. Wang, F. Sun, Y. Xie, X. Liu, J. Ma, X. Wang, C. Tian, J. Li, H. Fu, *Adv. Mater.* **2019**, *31*, 1901666.
[13] Y. Xu, P. Deng, G. Chen, J. Chen, Y. Yan, K. Qi, H. Liu, B. Y. Xia, *Adv. Funct. Mater.* **2019**, 1906081.
[14] I. S. Amiinu, X. Liu, Z. Pu, W. Li, Q. Li, J. Zhang, H. Tang, H. Zhang, S. Mu, *Adv. Funct. Mater.* **2018**, *28*, 1704638.
[15] S. Han, X. Hu, J. Wang, X. Fang, Y. Zhu, *Adv. Energy Mater.* **2018**, *8*, 1800955.
[16] Y. Jiang, Y.-P. Deng, J. Fu, D. U. Lee, R. Liang, Z. P. Cano, Y. Liu, Z. Bai, S. Hwang, L. Yang, D. Su, W. Chu, Z. Chen, *Adv. Energy Mater.* **2018**, *8*, 1702900.
[17] L. Wei, H. E. Karahan, S. Zhai, H. Liu, X. Chen, Z. Zhou, Y. Lei, Z. Liu, Y. Chen, *Adv. Mater.* **2017**, *29*, 1701410.
[18] C. Tang, B. Wang, H.-F. Wang, Q. Zhang, *Adv. Mater.* **2017**, *29*, 1703185.
[19] H. Yang, B. Wang, H. Li, B. Ni, K. Wang, Q. Zhang, X. Wang, *Adv. Energy Mater.* **2018**, *8*, 1801839.